Modeling and Cascade PID Controller Design of a Spinbath Circulation Process

Immanuel R. Santjoko, Tua A. Tamba*, and Ali Sadiyoko
Department of Electrical Engineering
Parahyangan Catholic University
Bandung, Indonesia
**Corresponding author*: ttamba@unpar.ac.id

***Abstract*—This paper reports the development of a cascade PID type control scheme for a MIMO spinbath circulation process regulation. In the proposed scheme, the dynamic model of the complete spinbath circulation process is first developed using concepts from fluid dynamics. Reduction of the obtained model through lumping of identical processes as well as linearization techniques is then conducted to obtain a simplified MIMO linear system with cascading control structure. A cascade PI control configuration is then constructed to achieve simultaneous control objectives in the interacting process variables of the developed simplified model [1]–[3]. More specifically, the proposed cascade controller is of the type of summed setpoint cascade PI that is selected for its cost-effectiveness and computational efficiency. It combines a summed setpoints to simultaneously manages multiple inputs, as well as cascades of faster inner disturbance rejection to allow for the minimization of the overall process' output deviations. Simulation results for constant as well as changing setpoints are then presented to demonstrate the effectiveness of the proposed modeling and cascade control schemes.**

***Index Terms*—Spinbath Circulation, Fluid Dynamics, Cascade PID Control**

I. Introduction

The spinbath circulation is a process that is often used in the production of viscose staple fiber (VSF). The VSF itself is a synthetic fiber derived from regenerated cellulose and is typically made from wood pulp [4]. In the VSF production process, the viscose solution is sprayed through a spinneret into the spinbath solution inside a spinning machine [5], [6]. As a result, the cellulose in the viscose solution coagulates to form filaments and other chemicals such as water, H_2S, and CS_2 [7]. Over time, the returned spinbath solution often gets diluted and contaminated, thereby requires some filtration and evaporation processes [8]. The recovery of the spinbath solution and its recirculation back to the spinning machine occurs in the spinbath circulation system. Hence, the design of control systems which appropriately regulate such a circulation process is necessary to ensure high-quality VSF production.

This paper reports the development of a cascade PID control scheme for a multi-input multi-output (MIMO) spinbath circulation process regulation. In the proposed scheme, the dynamic model of the complete spinbath circulation process is first developed using concepts from fluid dynamics. Reduction of the obtained model through lumping of identical processes and linearization techniques is then conducted to obtain a simplified MIMO linear system with a cascading control structure [9]. A cascade PID controller is constructed to achieve simultaneous control objectives in the interacting process variables of the developed simplified model. More specifically, the proposed cascade controller is of the type of summed setpoint cascade PID, selected for its cost-effectiveness and computational efficiency [10], [11]. It combines summed setpoints to manage multiple inputs and cascades faster inner disturbance rejection to reduce overall process output deviations [12], [13]. Simulation results are presented to illustrate the good performance of the proposed controller for setpoint regulation and disturbance rejection purposes.

The remainder of this paper is structured as follows. System configuration and problem formulation are discussed in section III. Section III briefly describes the spinbath circulation process and then derives its complete and simplified dynamic models. Cascade control schemes are proposed in section IV, and their performances are evaluated through simulations in section V. Section VI concludes the paper with final remarks.

II. System Description and Problem Formulation

A. Spinbath Circulation Scheme

This paper considers a simplified configuration of the spinbath circulation process as illustrated in Fig. 1. To develop the model, the steady-state equations are first derived using fluid

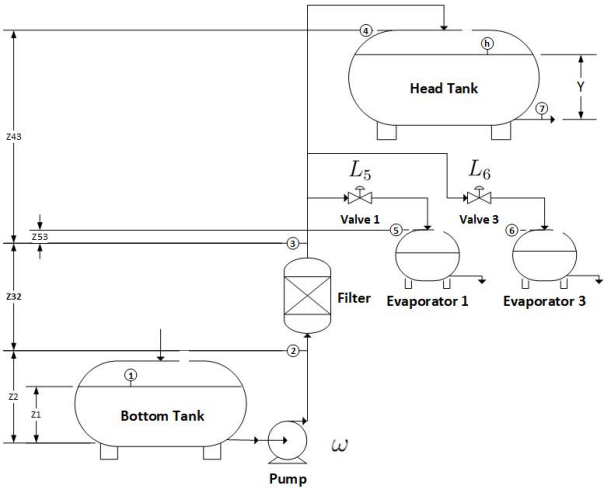

Fig. 1. Schematic of the spinbath circulation process.

dynamics' concept, and then linearized using an assumption that the system dynamics are of first order type. This modeling approach relies on estimated system parameters and dynamics.

Eight inspection points are used in modeling process, each with the following fluid characteristics: pressure (p), density (ρ), gravitational acceleration (g), velocity (V), and elevation gain (z). The system has three actuators: two control valves with evaporator 1 valve opening (L_5) and evaporator three valve openings (L_6), and one pump with angular speed (ω). There are three system outputs, namely: the head tank level (Y), evaporator 1 flow rate (Q_5), and evaporator 3 flow rate (Q_6) which is defined as the product between the velocity (V) and the cross-sectional area (A) of the channel.

B. Problem Formulation

In the considered system configuration, the pump's angular speed directly affects both the evaporator flow and the head tank level, while the control valve directly affects the evaporator flow and indirectly affects the head tank level. There are three control loops that are not interconnected to each other: one single-loop to regulate the head tank level, and two single-loop to regulate the evaporator flow. Thus, changes in the evaporator flow setpoint are viewed as a disturbance to the head tank inlet flow. This causes deviations in the head tank level, which then translate to deviations in the spinning machine flow rate, ultimately resulting in poor product quality.

III. System Modelling

Based on the schematic in Fig. 1, the model derivation is divided into several sections according to the main components of the system, namely: pump, filter, head tank flow, head tank level, evaporator 1, and evaporator 3.

A. Pump

The pump head (h_p) in the system is assumed to be approximated using the following equation [14]

$$h_p = A\omega^2 + B\omega Q - CQ^2 \tag{1}$$

where A, B, and C are pump head constants. From inspection points 1 and 2, the bottom tank pressure is known to be zero ($P_1 = 0$) as it is exposed to the atmospheric pressure. Additionally, the velocity at the bottom of the tank is assumed to be negligible ($V_1 \approx 0$) because the large tank area renders changes in velocity to be insignificant. Using steady flow energy assumption [15], the head of the pump satisfies (2).

$$\begin{aligned} \cancel{\frac{p_1}{\rho g}}^{\,0} + \cancel{\frac{V_1^2}{2g}}^{\,0} + z_1 &= \frac{p_2}{\rho g} + \frac{V_2^2}{2g} + z_2 - h_p + h_{f2} \\ h_P &= \frac{p_2}{\rho g} + z_{21} + \left(\frac{1}{2{A_2}^2 g} + k_2\right) Q^2 \end{aligned} \tag{2}$$

Combining (1) and (2), the equilibrium point $\mathbf{f}_1(p_2, \omega, Q)$ below can be obtained.

$$\mathbf{f}_1(p_2, \omega, Q) = \frac{p_2}{\rho g} - A\omega^2 - B\omega Q + \left(C + \frac{1}{2{A_2}^2 g} + k_2\right) Q^2$$

Assuming (1,1,1) to be the equilibrium point $\mathbf{f}_1$, the linearized dynamics which ignores higher order terms thus satisfy (3).

$$\mathbf{L}_1(p_2, \omega, Q) = c_1 \delta p_2 - c_2 \delta\omega + c_3 \delta Q \tag{3}$$

where $c_1 = 1/\rho g$, $c_2 = 2A{+}1$, and $c_3 = B{+}2C{+}2/(2{A_2}^2 g)$. Assuming further that the transient response of the model is of first-order type, the constant c_2/c_1 can be represented as a transfer function G_1, while c_3/c_1 can be represented as another transfer function G_2. Specifically, G_1 is assumed to be of the form $\alpha_1/(\tau_1 s + \beta_1)$ and G_2 is of the form $\alpha_2/(\tau_2 s + \beta_2)$. Therefore, the model of the pump can be written as follows.

$$\delta p_2 = G_1 \delta\omega - G_2 \delta Q \tag{4}$$

Here, we use $\alpha_1 = \beta_1 = \beta_2 = \tau_1 = \tau_2 = 1$, and $\alpha_2 = 0.2$.

B. Filter

From inspection points 2 and 3, the inlet velocity (V_2) and the outlet velocity (V_3) of the filter are assumed to be the same, thereby cancel each other out in the energy balance equation. Using steady flow energy equation [15], the head of the filter system equilibrium $\mathbf{f}_2(p_2, p_3, Q)$ satisfies the equation below.

$$\begin{aligned} \frac{p_2}{\rho g} + \cancel{\frac{V_2^2}{2g}}^{\,0} + z_2 &= \frac{p_3}{\rho g} + \cancel{\frac{V_3^2}{2g}}^{\,0} + z_3 + h_{f3} \\ \mathbf{f}_2(p_2, p_3, Q) &= -\frac{p_2}{\rho g} + \frac{p_3}{\rho g} + z_{32} + k_3 Q^2 \end{aligned} \tag{5}$$

Again, assuming (1,1,1) as an equilibrium point for $\mathbf{f}_2$, the corresponding linearized dynamics can be expressed as [16]

$$\mathbf{L}_2(p_2, p_3, Q) = -c_4 \delta p_2 + c_5 \delta p_3 + c_6 \delta Q \tag{6}$$

By further assuming that the transient response of the model is of first-order type, the constant c_{10}/c_9 can be represented as a transfer function G_7. Specifically, G_3 is given by $\alpha_3/(\tau_3 s + \beta_3)$ and G_4 by $\alpha_4/(\tau_4 s + \beta_4)$. Thus, the filter model can be written as (7) in which $c_4 = 1/\rho g$, $c_5 = 1/\rho g$, and $c_6 = 2k_3$.

$$\delta p_3 = G_3 \delta p_2 - G_4 \delta Q \tag{7}$$

Here, we use $\alpha_3 = \beta_3 = \beta_4 = \tau_3 = \tau_4 = 1$, and $\alpha_4 = 0.2$.

C. Head Tank Flow

Using the law of mass conservation, the total mass flow rate into the system $\Sigma \dot{m}_i$ equals the total mass flow rate out of the system $\Sigma \dot{m}_o$. Assuming that the fluids are of incompressible type, the relationships in (8) may then be formulated.

$$\begin{aligned} \dot{m}_3 &= \dot{m}_4 + \dot{m}_5 + \dot{m}_6 \\ \rho Q_3 &= \rho_4 Q_4 + \rho_5 Q_5 + \rho_6 Q_6 \\ Q &= Q_4 + Q_5 + Q_6 \end{aligned} \tag{8}$$

From inspection points 3 and 4, the pressure in the head tank is assumed to be zero ($p_4 = 0$) as it is exposed to atmospheric pressure. Furthermore, the inlet velocity of the head tank (V_4) is assumed to be equal to the outlet velocity of the filter (V_3). This means that they cancel each other out

in the energy equation. Based on steady flow energy equation [15], the equilibrium $\mathbf{f}_3(p_3, Q_4)$ of the head tank flow satisfies

$$\begin{aligned} \frac{p_3}{\rho g} + \cancelto{0}{\frac{{V_3}^2}{2g}} + z_3 &= \cancelto{0}{\frac{p_4}{\rho g}} + \cancelto{0}{\frac{{V_4}^2}{2g}} + z_4 + h_{f4} \\ \mathbf{f}_3(p_3, Q_4) &= -\frac{p_3}{\rho g} + z_{43} + k_4 {Q_4}^2 \end{aligned} \tag{9}$$

Assuming (1,1) to be the equilibrium $\mathbf{f}_3$, the linearized dynamics around this equilibrium can be expressed as follows.

$$\mathbf{L}_3(p_3, Q_4) = c_7 \delta p_3 + c_8 \delta Q_4 \tag{10}$$

where $c_7 = 1/\rho g$ and $c_8 = 2k_4$. Assuming that the transient response of the model is of first-order type, the constant c_8/c_7 can be represented as a transfer function $G_5 = \alpha_5/(\tau_5 s + \beta_1)$. Therefore, the head tank flow model can be written as

$$\delta Q_4 = G_5 \delta p_3 \tag{11}$$

where $\alpha_5 = \tau_5 = \beta_5 = 1$ are assumed.

D. Head Tank Level

Assuming mass conservation [15], the change of mass in the head tank ($\dot{m}_h$) is influenced by the difference between the mass entering the head tank ($\dot{m}_4$) and the mass leaving the head tank ($\dot{m}_7$). If the mass leaving the head tank ($\dot{m}_7$) is constant, the head tank level can be modeled as follows.

$$\begin{aligned} \frac{dm}{dt} &= \dot{m}_4 - \dot{m}_7 \\ \rho A \frac{dy}{dt} &= \rho (Q_4 - Q_7) \\ Y(s) &= (Q_4(s) - Q_7(s))\, G_6 \end{aligned} \tag{12}$$

with $G_6 = \alpha_{10}/\tau_{10} s$ with $\alpha_{10} = 1$ and $\tau_{10} = 10$ are assumed. The pressures in the head tank and the spinning machine are zero ($p_4 = p_7 = 0$) because they are open to and have direct contact with the atmospheric pressure. The velocity at the head tank is further assumed to be negligible (V_h) because the large tank area renders the changes in level to be insignificant.

Using steady flow energy assumption [15], the equilibrium of the head tank level system can be defined as in (13).

$$\begin{aligned} \cancelto{0}{\frac{p_h}{\rho g}} + \cancelto{0}{\frac{{V_h}^2}{2g}} + z_h &= \cancelto{0}{\frac{p_7}{\rho g}} + \frac{{V_7}^2}{2g} + z_7 - h_p + h_{f7} \\ \mathbf{f}_4(Y, Q_7) &= -Y + \left(\frac{1}{2{A_7}^2 g} + k_7 \right) {Q_7}^2 \end{aligned} \tag{13}$$

Assuming (1,1) to be the equilibrium point $\mathbf{f}_4$, the linearized dynamics around this equilibrium satisfies the following.

$$\mathbf{L}_4(Y, Q_7) = -c_9 \delta Y + c_{10} \delta Q_7 \tag{14}$$

where $c_9 = 1/\rho g$ and $c_{10} = 2/(2{A_7}^2 g) + 2k_7$. Further assuming that the model's transient response is of first-order type, the constant c_{10}/c_9 is represented as a transfer function of the form $G_7 = \alpha_7/(\tau_7 s + \beta_7)$ in which the values $\alpha_7 = \tau_7 = \beta_7 = 1$ are assumed. Therefore, the head tank level model can be written as follows.

$$\delta Q_7 = G_7 \delta Y \tag{15}$$

E. Evaporator

For the evaporator system, the inlet velocity (V_3) and the outlet velocity (V_5) are assumed to be the same and thus cancels each other out in the energy balance equation. It is also assumed that the control valve response is a linear function of the form ($F_{(L_5)} = 1/L_5$), the pressure within evaporator 1 (p_5) remains constant, and the pipe resistance is negligible. Based on steady flow energy equation [15], the head's equilibrium of the evaporator system satisfies the following equation.

$$\begin{aligned} \frac{p_3}{\rho g} + \frac{{V_3}^2}{2g} + z_3 &= \frac{p_5}{\rho g} + \cancelto{0}{\frac{{V_5}^2}{2g}} + z_5 + h_{f5} \\ \mathbf{f}_5(p_3, L_5, Q_5) &= -\frac{p_3}{\rho g} + \frac{p_5}{\rho g} + z_{53} + (k_5 + F_{(L_5)}) {Q_5}^2 \\ &= -\frac{p_3}{\rho g} + \frac{p_5}{\rho g} + z_{53} + \frac{1}{L_5} {Q_5}^2 \end{aligned} \tag{16}$$

Assuming (1,1,1) to be the equilibrium point $\mathbf{f}_5$, the linearized dynamics around this equilibrium satisfies the following.

$$\mathbf{L}_5(p_3, L_5, Q_5) = -c_{11} \delta p_3 + c_{12} \delta L_5 + c_{13} \delta Q_5 \tag{17}$$

where $c_{11} = 1/\rho g$, $c_{12} = 1$, and $c_{13} = 2$. If the model's transient response is of first-order type, the constant c_{11}/c_{13} can be represented as a transfer function G_8 and c_{12}/c_{13} is represented as the transfer function G_9. Specifically, G_8 is given by $\alpha_8/(\tau_8 s + \beta_8)$ and G_9 by $\alpha_9/(\tau_9 s + \beta_9)$, respectively, where $\alpha_8 = \alpha_9 = \beta_8 = \beta_9 = 1$ and $\tau_8 = \tau_9 = 3$ are assumed. Thus, the evaporator 1 can be modeled as follows.

$$\delta Q_5 = G_8 \delta p_3 + G_9 \delta L_5 \tag{18}$$

If evaporators 3 and 1 are assumed to have the same parameters, then (19) can be obtained with $G_{10} = G_8$ and $G_{11} = G_9$.

$$\delta Q_6 = G_{10} \delta p_3 + G_{11} \delta L_6 \tag{19}$$

F. System Block Diagram

Based on the aforementioned modeling, the block diagram of the system model as shown in Fig. 2 can be constructed. Note in this figure that the system model has three inputs, namely the pump's angular speed (ω), evaporator 1's valve

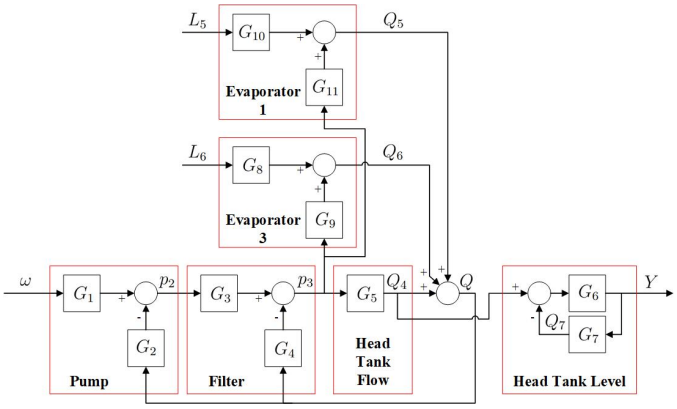

Fig. 2. Block diagram of the system model.

opening (L_5), and evaporator 3's valve opening (L_6). Since the evaporator flow rates are not critical for the control objectives, the output in the simplified model is set to be head tank's level (Y). Notice that the evaporators' valve opening indirectly affect the head tank's level negatively through the corresponding decrease in pump and filter pressures.

IV. Control System Design

Based on Fig. 2, three control configurations for head tank level regulation were developed: (i) single-loop, (ii) cascade, and (iii) summed setpoint cascade controllers.

A. Single-loop Control System

This controller is shown in Fig. 3 which includes one single-loop controller (C_1) to regulate the head tank level with R as its setpoint, and two additional single-loop controllers C_6 and C_7 to regulate the flows of evaporator 1 and evaporator 3 with setpoint values of D_1 and D_2, respectively. All controllers are of PID types. The head tank level controller adjusts the pump angular speed, which directly affects both the head tank level and the evaporator flow rate positively. Since the evaporator flow rates are not critical for the control objectives, minor variations are assumed to be acceptable in the present study.

B. Conventional Cascade Control System

To address the single-loop control limitation, a cascade control system as shown in Fig. 4 is proposed to regulate the head tank level. The outer loop controller (C_2) regulates the head tank level (Y) with R as a setpoint, while the inner loop controller (C_3) regulates the head tank flow rate (Q_4)through the pump's angular speed adjustment. As in the single-loop case, all controllers in this configuration are also of PID types.

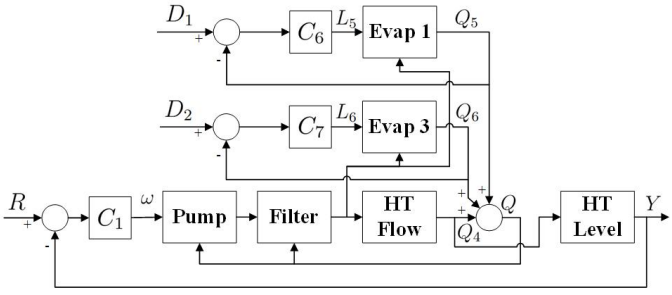

Fig. 3. Block diagram of the single-loop control system.

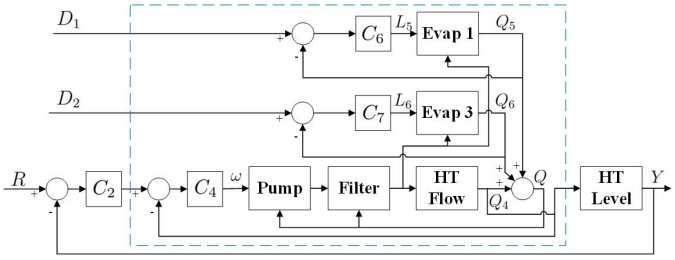

Fig. 4. Block diagram of the conventional cascade control system.

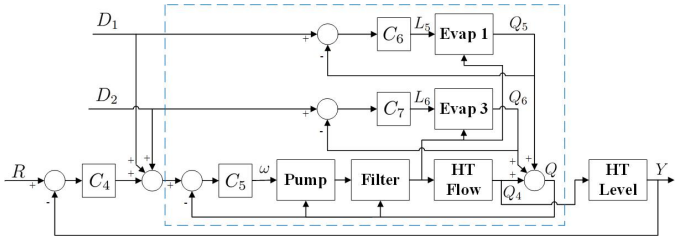

Fig. 5. Block diagram of the summed setpoint cascade control system.

C. Summed Setpoint Cascade Control System

A summed setpoint cascade control system is finally proposed to to address the prior two controllers. The outer loop controller (C_4) regulates the head tank level (Y) with R as its setpoint, while the inner loop controller (C_5) regulates the total flow rate (Q). The inner loop controller also adjusts the pump angular speed. All controllers in this configuration utilize are of PID types, and the resulting block diagram of the cascade control system is depicted in Fig. 5.

V. Simulation Results

Simulations were performed in MATLAB [17] to evaluate the performance of the three control configurations. In each scheme, the PID control tuning is performed from the innermost to the outermost control blocks [13]. The tuning is performed using MATLAB's PID Tuner toolkit with suitable adjustment on closed loop response times to achieve the best response results [18]. The chosen tuning results in a robustness index of 0.7 and a response time ratio between the inner and outer controllers of 1:2.5. The resulting PID parameters as summarized in Table I suggest that a PI controller is sufficient for each control structure. More detailed simulation results for each control scheme are discussed as follows.

A. Step Response Simulation Result

Two simulations were conducted to analyze the step responses of the closed loop simplified spinbath circulation models in Figs. 3, 4, and 5 for inputs R and D_1. Zero initial conditions and a sampling time of $T_s = 70$s are used. Fig. 6 plots the step response of the closed loop system for all controllers for input signal R, while Fig. 7 plots the response to

TABLE I
PID parameters of the closed loop systems.

Controller	System Parameter		PID Parameter		
	Response Time	Transient Behavior	K_p	K_i	K_d
C_1	20s	0.7	1.2277	0.1565	0
C_2	8s	0.7	0.9687	0.0971	0
C_3	20s	0.7	0.3224	0.3519	0
C_4	8s	0.7	0.9687	0.0971	0
C_5	20s	0.7	0.3224	0.3519	0
C_6 & C_7	3	0.7	1.2321	1.2440	0

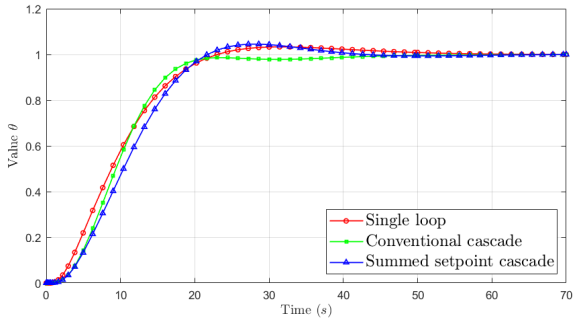

Fig. 6. Step responses of all controllers to input R.

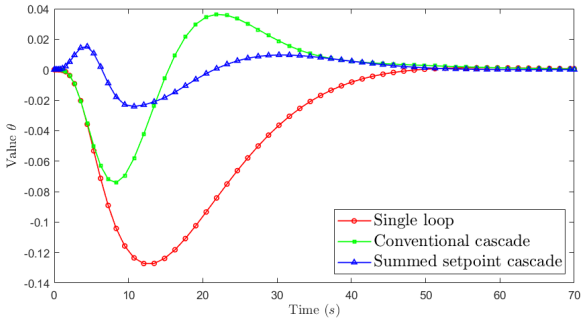

Fig. 7. Responses of all controllers to disturbance input D.

TABLE II
STEP RESPONSES AND IAE OF DIFFERENT CONTROL STRUCTURES

Information	**single-loop**		**Conv. Cascade**		**S.S. Cascade**	
	R	D	R	D	R	D
Rise Time	13.90	-	11.80	-	13.35	-
Settling Time	35.16	20.38	20.06	44.28	26.32	36.74
Peak Max	1.033	0.001	1	0.036	1.045	0.015
Peak Min	-	-0.127	-	-0.074	-	-0.024
IAE	10.24	2.599	10.30	1.153	11.40	0.443

disturbance signal D. From these plots, the resulting response characteristics as well as integral absolute error (IAE) values are extracted and then summarized in Table II.

Fig. 6 shows that all three control schemes produce closely similar step response characteristics to the input signal R. The responses in this plot also reveal that the peak and integral absolute error (IAE) values differ only slightly among the three control schemes. All control schemes exhibit overshoots within tolerable values of less than 10%, with the conventional cascade control system demonstrating slightly superior performance in terms of rise time and settling time criteria.

As for the responses to disturbance signal D in Fig. 7, the conventional and summed setpoint cascade controllers show better performances when compared to the single-loop control system in terms of minimizing the response deviation. This thus suggests that cascade controllers significantly outperform the single-loop controller in terms of disturbance rejection capability. Specifically, the peak value in the summed setpoint cascade control system is reduced by approximately 81%,

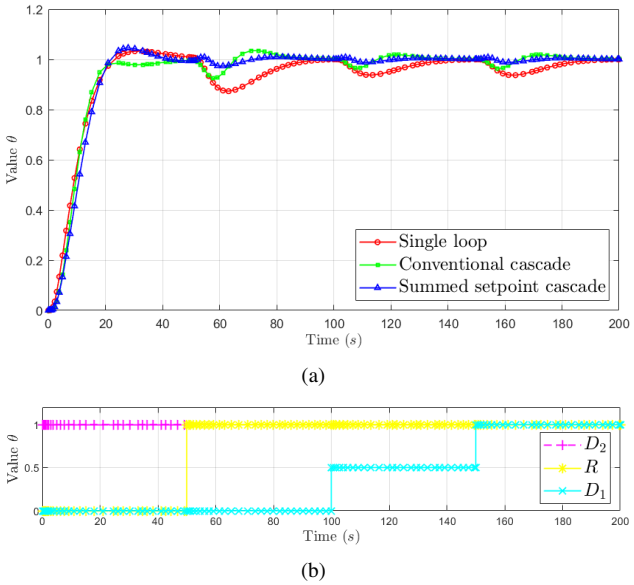

Fig. 8. System response for changing setpoints: (a) response, (b) setpoint.

indicating a much smaller deviation from the desired output in the presence of disturbances. Additionally, the resulting IAE of the summed setpoint cascade control system is reduced by 83%, which highlights substantial improvement in terms of maintaining adherence to the setpoint over time. While the conventional cascade control system also shows improvements by reducing both the peak value and IAE, the summed setpoint cascade control system surpasses it in overall performance.

B. Multiple-Input Simulation Result

In real-world scenarios, simultaneous setpoint changes are often occurred or required to be done. Thus, simulation evaluation for multiple inputs' case were also conducted to comprehensively evaluate the system performance. The simulation were conducted with zero initial condition and a sampling time of $T_s = 200$s. The inputs were set to be step functions that are delayed up to times $T = 0$ for input signal R and $T = 50$ for input D_1, respectively, as well as two successive 0.5 increment step functions that are delayed up to times $T = 100$ and $T = 150$, respectively, for input signal D_2.

Fig. 8(a) plots the closed loop system responses for all control schemes with respect to a series of setpoint changes that are shown in Fig. 8(b). This plot shows that the system characteristics remain similar to those observed in the case of single step input response. The IAE value is 15.34 for the case of using single-loop controller, 12.55 for the case of using conventional cascade controller, and 12.28 for the case of using summed setpoint cascade controller. These thus indicate the better performance of the summed setpoint controller. In real-life applications, there is often a tolerable maximum deviation value, and the evaporator flow setpoint changes more frequently than the head tank level setpoint. As a result, the summed setpoint can use larger time steps, while the single-loop controller requires smaller, more frequent adjustments.

VI. Conclusion

This paper has presented the modeling and cascade controller design of a MIMO spinbath circulation process. The model is constructed using concepts from fluid dynamics, while the cascade control scheme is designed using the summed setpoint cascade PI structure. Simulation results for constant and changing setpoint values are also reported to demonstrate the effectiveness of the proposed modeling and control schemes. In the future, we aim to replace the assumed model with a data-driven model that is estimated from real-time operational data using system identification method. The use of such a model is expected to further enhance the accuracy and practicality of the proposed control strategy.

VII. Acknowledgement

This work was supported by Ministry of Education, Culture, Research, and Technology (Kemendikbudristek) of Republic of Indonesia through Fundamental Research grant year 2024.

References

[1] V. Dubey, H. Goud, and P. C. Sharma, "Role of pid control techniques in process control system: a review," *Data Engineering for Smart Systems: Proceedings of SSIC 2021*, pp. 659–670, 2022.

[2] M. Ferrari and A. Visioli, "An educational interactive software tool to learn cascade control design," *IFAC-PapersOnLine*, vol. 56, no. 2, pp. 7561–7566, 2023.

[3] K. Chandran *et al.*, "Modified cascade controller design for unstable processes with large dead time," *IEEE Access*, vol. 8, pp. 157 022–157 036, 2020.

[4] J. Chen, "Synthetic textile fibers: Regenerated cellulose fibers," in *Textiles and Fashion (Ch. 4)*, ser. Woodhead Publishing Series in Textiles, R. Sinclair, Ed. Woodhead Publishing, 2015, pp. 79–95.

[5] V. Gupta, "Solution-spinning processes," in *Manufactured fibre technology*. Springer, 1997, pp. 124–138.

[6] A. G. Wilkes, "The viscose process," *Regenerated cellulose fibres*, pp. 37–61, 2001.

[7] I. S. Mendes, A. Prates, and D. V. Evtuguin, "Production of rayon fibres from cellulosic pulps: State of the art and current developments," *Carbohydrate Polymers*, vol. 273, p. 118466, 2021.

[8] APR, *Asia Pacific Rayon: Process and Technical Description Modules*, Asia Fibre Trading Pte Ltd, Accessed on: 2020.

[9] R. B. Sartor, J. O. Trierweiler, and P. R. B. Fernandes, "Obtaining linearized dynamic models from steady-state simulations," in *Seminario do Programa de Pos-Graduacao em Engenharia Quimica (10.: 2011 out. 04-07: Porto Alegre, RS)*, 2011, pp. 1–6.

[10] R. Nian, J. Liu, and B. Huang, "A review on reinforcement learning: Introduction and applications in industrial process control," *Computers & Chemical Engineering*, vol. 139, p. 106886, 2020.

[11] L. Liu, S. Tian, D. Xue, T. Zhang, Y. Chen, and S. Zhang, "A review of industrial mimo decoupling control," *International Journal of Control, Automation and Systems*, vol. 17, no. 5, pp. 1246–1254, 2019.

[12] A. Celna *et al.*, "Centralized frequency control of offshore hybrid power plant," in *Proc. 8th International Hybrid Power Plants & Systems Workshop*, 2024, pp. 106–114.

[13] R. Vilanova and O. Arrieta, "PID tuning for cascade control system design," in *Proc. Canadian Conference on Electrical and Computer Engineering*, 2008, pp. 001 775–001 778.

[14] G. Janevska, "Mathematical modeling of pump system," in *Electronic International Interdisciplinary Conf.*, vol. 2, 09 2013, pp. 455–458.

[15] F. White, *Fluid Mechanics*. McGraw-Hill Education, 2015.

[16] K. Ogata, *Modern Control Engineering*. Prentice Hall, 2010.

[17] MATLAB, *ver. R2020a*. Natick, MA, USA: The MathWorks Inc., 2020.

[18] L. Wang, *PID control system design and automatic tuning using MATLAB/Simulink*. John Wiley & Sons, 2020.